https://erjm.journals.ekb.eg
ISSN: xxxx-xxxx

DOI: ---------

ERJ
Engineering Research Journal
Faculty of Engineering
Menoufia University

Numerical and Experimental Investigation of the Ducted Wind Turbine Performance With and Without Obstacle Plates

Mohamed A. Abdelmordy, Ali M. Abdelsalam, Ismail M. Sakr *, Kamal A. Ibrahim
** Mechanical Power Engineering Department, Faculty of Engineering, Menoufia University, Shebin El-Kom, Egypt.*
(Corresponding author: ismailsakr@yahoo.com)

ABSTRACT
Obstacle plates of various designs were used in previous studies to enhance the performance of the Savonius rotor operating in free wind conditions. The present work is aimed to investigate an obstacle plate upstream wind turbine installed inside a duct. Installing wind turbines in a through-building channel provides a great opportunity for wind speed augmentation and consequently harvesting more power from the wind. In this case, as the free wind is redirected into the duct which makes the flow towards the rotor unidirectional; the obstacle plat is expected to decrease the negative effect on the wind turbine operation. On the contrary, the net driving force can be enhanced by reducing the reverse force on the convex blade. Furthermore, the static torque which is a measure of the rotor starting ability can be improved. The rotor performance is numerically and experimentally investigated in free wind conditions and inside the duct with and without obstacle plates. The results showed a higher power coefficient (C_p) for the ducted rotor with C_{Pmax} = 0.188 as compared to the free wind rotor of C_{Pmax} = 0.165. Moreover, introducing obstacle plates upstream of the rotor with an angle of α=35º to the main flow direction increases the rotor performance, with C_{Pmax} = 0.216. The increase in rotor power coefficient records 15% and 31% as compared to the rotor without obstacle plate and rotor in free wind conditions, respectively. The static torque in the case of obstacle plates of α=35º has positive values at all rotor orientations (rotation angles) which ensures good starting ability of the present Savonius rotor operation.

Keywords: *Savonius Rotor; Obstacle plate; Free jet; Power coefficient; Ducted Turbine*

1. Introduction

Renewable energy resources such as hydropower, solar energy, biomass, and wind energies are starting to play an important role in the energy sectors due to pollution of carbon dioxide from fossil fuels in addition to depletion of the conventional resources. Wind energy is a highly suitable energy resource that can be used for this purpose. Wind turbines can be classified based on their rotational axis orientation, with respect to the wind direction. In this case, there are two types of wind turbines; horizontal axis wind turbine (HAWT) and vertical axis wind turbine (VAWT).

Savonius rotor is a drag type of VAWT which has simple structure because it is composed mainly of two vertical half cylinders. Moreover, it has many advantages like low self-starting, low noise, ability to work at low wind speed and the adaption to operate in highly turbulent flow [1-3]. However, it suffers from low efficiency compared to other turbines. Many studies including experimental and numerical investigations were carried out considering the geometrical parameters of the rotor [4]. One of the significant parameters affecting the turbine performance is the overlap ratio. The Savonius rotor with 0.15 overlap ratio would generally have the highest power coefficient [5-6]. Furthermore, two-bladed rotors were more efficient than three bladed rotors [7]. Jeon et al [8] proved that using end plates also enhanced the rotor performance.

One of the factors of degradation the C_p of the Savonius turbine is the negative torque produced by the convex returning blade. Placing an obstacle plate, also called wind shields or deflectors, upstream the convex blade can decrease the flow resistance confronted by the returning blade. Moreover, the essential goal of using those geometries is to reduce the drag force of the convex blade in which the wind pressure generates a negative torque. Furthermore, the drag force will be propagated on the concave

blade. These methods show a valuable result in increasing the starting characteristics of the rotor as well as the C_p [4-9]. Several obstacle plate designs have been developed over the last few decades. Ogawa et al. [10] investigated experimentally the effect of an obstacle plate before the returning blade with various adjustable angles. They concluded that the obstacle plate with an angle of 30º under their configuration improved the C_p by 27% compared to a bare Savonius rotor. Shaughnessy and Probert [11] carried out experimental study on two blade Savonius rotor with V-shape obstacle plate placed upstream the returning blade. It was found that the optimal angle between two blades of the plate was 37º. This configuration gave increase in C_p by 20%. Moreover, the range of tip speed ratio expanded about 2.3 greater than that for bare rotor. Recently, Etemadeasl et al. [12] carried out numerical investigations on V-shape obstacle plate upstream two counter rotating Savonius rotors. Their results showed 80% increase in C_p with an obstacle angle of 90º. Shouichiro et al. [13] studied the effect of an obstacle plate placed upstream of a hydraulic Savonius turbine. The performance increased by 80% under 0.73 clearance ratio. Kailash et al. [14-15] investigated the effect of obstacle plate on the performance of modified Savonius rotor in water medium. The results showed that the maximum C_p reached up to 0.21 which increased by 50% where optimizing the position of the obstacle plate upstream the returning rotor blade. The operating tip speed ratio λ was slightly increased. Under water medium also, Golecha et al. [16] investigated experimentally the influence of the deflector plate on the performance of modified Savonius rotor. The maximum C_p was improved by 42% and 31% with deflector plate for two stages 0º phase shift and 90º phase shift, respectively.

Aboujaoude et al. [17] presented a new type of deflector for the Savonius wind turbine to improve its performance. This deflector is an axisymmetric truncated cone, designed and optimized by a numerical method. This new deflector allows to reach a value of $C_{p_{max}} = 0.31$ and thus to increase the performance of the wind turbine by 25% in all wind configurations. On the other hand, Wahyudi et al. [18] recommended using a moving deflector plate around Savonius which increased the velocity towards the advancing plate and enhanced the performance. Roy et al. [19] experimentally studied the change of deflector plate angle upstream the advancing blade and the returning blade in a wind tunnel. The results showed that under optimum angle of the deflectors' the C_p was around 0.41 for newly developed Savonius Style turbine. It is worth noting that, as the wind tunnel is fed with constant mass flow rate and is confined, directly the flow to the advancing blade will certainly increase the positive torque of the rotor. However, this is not the case when installing obstacle plate upstream the wind turbine in free wind. The opportunity for the flow to escape from lateral sides may eliminate the advancing of installing obstacle plate. Altan et al. [20] suggested new design containing two certain plates under experimental and numerical investigations. They claimed that the improvement in the extracted power was 16 % with 45º and 15º angles of certain plates. El-Askary et al. [21] suggested numerically a new design of three fixed plates to direct the wind to the returning blade on the other surface of the same blade. The results showed that the maximum C_p of the design reached up to 0.52. However, they noticed a strong vortex shedding was generated. Mohamed et al. [22] carried out automatic optimizations with numerical simulations by ANSYS fluent to investigate the superior angle of obstacle shielding before returning blade for two and three bladed Savonius rotor. They claimed that 100.8º was the superior angle for two-bladed and 80.52º for three-bladed Savonius turbine. Under this configuration, the C_p reached up to 0.27 with an enhancement in the performance of 40% compared to free stream conventional Savonius rotor [23].

Exploring the performance of wind turbines enclosed by shroud or duct is more important for those rotors installed inside a through-building channel. This is beneficial for wind speed enhancement and consequently power output from the wind rotor which may exceed the Betz limit [24]. Lawn [25] developed one-dimensional theory to predict the performance of wind turbine in duct. The results showed that the enhancement in performance reached up to 30% compared to a bare turbine. Mishra et al. [26] investigated experimentally the effect of duct on Savonius rotor. They observed a significant increase in power generation. Bai et al. [27] investigated numerically the influence of channel on the performance of Savonius rotor. The results showed that the double rotor diameter was the optimum width of the channel. Furthermore, they also predicted a mathematical equation to obtain the Savonius maximum C_p through the channel. Mauro et al. [28] carried out experimental data as well as a 2D CFD model to predict the blockage effect on shrouded Savonius turbine. A strong overpressure upstream of the turbine was generated by the blockage influence, which represented another source to generate energy. They concluded that the C_p of ducted turbine increased to around double fold.

It is concluded from this review that placing obstacle plates upstream wind turbine in open space has great effect on the performance improvement. However, testing obstacle plate upstream wind turbine encased by a duct is rare in literature. Hence, it is aimed in the present work to investigate the performance of Savonius wind turbine encased by a duct utilizing obstacle plate of different angles. A comparison with wind turbine in open space is also compared. Exploring the performance in that case is more important for wind turbines operating in a through-building channel.

2. Physical Model of Duct and Savonius Rotor

Figure 1 shows a schematic representation of the Savonius rotor surrounded by the duct. A Savonius rotor of 40 cm diameter is placed at centreline of 60 cm x 80 cm duct cross section with a duct length 300 cm in the axial direction. Double rotor diameter is chosen to be the duct width [28]. An obstacle plate of angle α to the duct wall is fixed upstream the Savonius rotor, facing a part of the returning blade. The angle α is allowed to vary in the present work, which keeping the obstacle projected length in the axial direction is kept as 40 cm. The Savonius turbine examined in this research is a conventional rotor shown in Fig. 2. The rotor has a diameter D of 40 cm width with an aspect ratio of one. The overlap ratio (δ=e/d) is chosen in the present study to be δ=0.15 [5-6]. The end plate diameter Do is 10% greater than the rotor diameter.

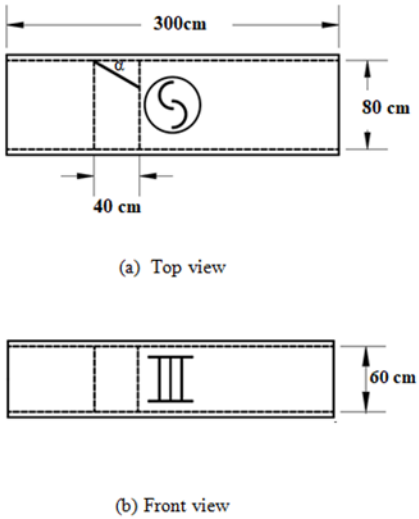

Fig. 1. Schematic diagram of ducted Savonius wind turbine

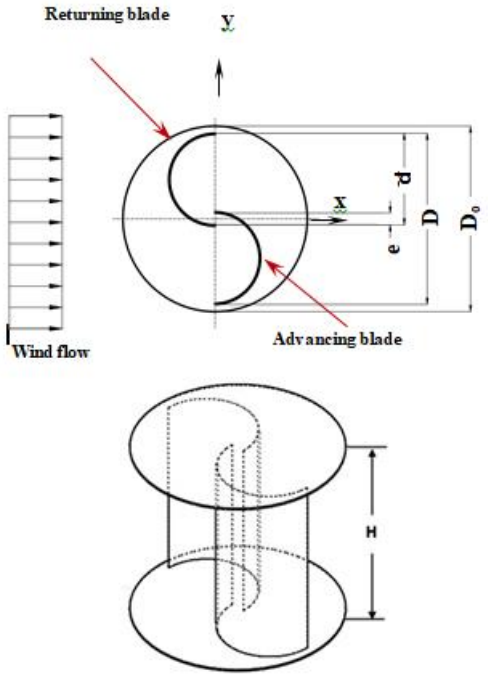

Fig. 2. Conventional Savonius rotor model.

3. Experimental Setup and Method of Measurement

To investigate experimentally the performance of wind turbine in free stream or inside a duct, a free jet test rig was designed and installed at the advanced fluid mechanics laboratory of the Faculty of Engineering at Menoufia University, Egypt. A schematic representation of the test rig used in the present work is shown in Fig. 3. It consists mainly of two parts. The first part is the wind source, which generates wind by a centrifugal fan driven by an AC motor. This wind source was initially used by [29] to study the performance of a twisted modified Savonius rotor and then modified and used in [30] to study the performance of horizontal axis wind turbine. The motor is controlled by an inverter which is used to adjust the motor rotational speed and consequently the fan rotational speed. Hence, different values of wind speeds are obtained by changing the fan rotational speed. The second part of the test rig is the duct evolving the wind rotor. The duct is placed in front of the free jet. Figure 4 shows a photograph of the Savonius rotor inside the duct with an obstacle plate and the rotor is placed at the middle of the duct. The rotor blades are installed in a steel shaft. Two ball bearings are placed on the frame for the shaft installation. The wind speed is measured by a digital regular Pitot tube EXTECH (Extech, HD350, USA), with an accuracy of ± 0.03 m/s and resolution of 0.01 m/s. The measurements are recorded vertically and horizontally through the

projected area of the rotor with a fixed step 10 cm. Hence, the average wind speed V is calculated taking into account the area weighted averaged of the measured wind speed. The wind speed is measured at least 5 times for the same case to achieve the repeatability of measurement. To obtain the rotational speed of the wind turbine rotor in (rpm) and the mechanical torque in (N.m), digital torque meter (AEP, MO.RT2M-TOR.541.R4, Italy) with range 0:25 N.m and accuracy of 0.001 N.m is used. The torque meter is coupled to a weighing pan and the rotor. The weight in the weighing pan is varied to change the brake torque and consequently the rotor rotational speed.

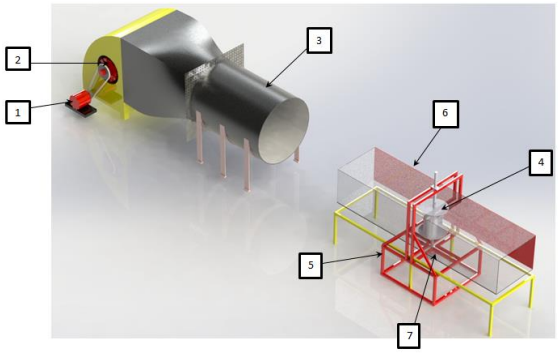

Fig. 3. Test rig of the current work: (1) AC motor, (2) Centrifugal fan, (3) Circular duct [30]; (4) Savonius rotor (5) Steel housing (6) Duct (7) Torque meter.

Fig. 4. A photograph for the test rig of the Savonius rotor inside duct with obstacle plate

4. Numerical methodology

The CFD simulations are employed in the present work to investigate the flow field around the ducted Savonius turbine. The finite volume method (FVM) has been utilized for discretizing the governing equations in ANSYS Fluent 17 [31]. The semi-Implicit Method for Pressure-Linked Equation (SIMPLE) is employed for the pressure-velocity coupling. The Reynolds Averaged Navier–Stokes (URANS) equations are implemented. For appropriate analysis, the sliding mesh model is employed to represent the rotation of the Savonius wind turbine. The flow variables are calculated from the conservation equations of momentum and mass. The general equation formulation for momentum conservation, employed in the present simulations, is expressed as follows:

$$\rho \frac{d}{dt} \int \varphi \, dV_{ol} + \rho \int \varphi \left(\vec{u} - \overrightarrow{u_g} \right). d\vec{A} = \int \Gamma \nabla \varphi . d\vec{A} + \int S_\varphi \, dV_{ol} \quad (1)$$

Where, ρ is the fluid density and φ is the general scalar representing components of the relative velocity $(\vec{u} - \overrightarrow{u_g})$ in *x*, *y*, and *z* directions. $\overrightarrow{u_g}$ is the velocity of moving mesh while $\vec{u}$ is the flow velocity vector. Γ is the diffusion coefficient, but S_φ is the source term, dVol is the cell volume. The general mass conservation equation is formulated as;

$$\nabla . \left(\vec{u} - \overrightarrow{u_g} \right) = 0 \quad (2)$$

4.1. Turbulence Modeling

The wind flow around the Savonius turbine is described by its turbulent fluctuating velocity fields. These fluctuations mix transported quantities such as energy and momentum, and cause the transported quantities to fluctuate as well. The inclusion of the Reynolds stress tensor in the momentum equations increases the number of unknown terms as compared to number of equations. So, turbulence modeling is inserted to calculate the additional tensors of URANS equations, by means of turbulent viscosity μ_t In the present work, renormalization group (RNG) *k*–ε turbulence is recommended for investigating the flow around Savonius turbine [32-33]. The transport equations for turbulence kinetic energy *k* and turbulence dissipation rate ε of the RNG *k*–ε model are formulated as follows;

$$\frac{\partial k}{\partial t} + \frac{\partial k u_i}{\partial x_i} = \frac{1}{\rho} \frac{\partial}{\partial x_j} \left[\sigma_k \mu_{eff} \frac{\partial k}{\partial x_j} \right] + G_k - \varepsilon + S_k \quad (3)$$

$$\frac{\partial \varepsilon}{\partial t} + \frac{\partial \varepsilon u_i}{\partial x_i} = \frac{1}{\rho} \frac{\partial}{\partial x_j} \left[\alpha_\varepsilon \mu_{eff} \frac{\partial \varepsilon}{\partial x_j} \right] + C_{1\varepsilon} \frac{\varepsilon}{k} (G_k) - C_{2\varepsilon}^{*} \frac{\varepsilon^2}{k} \quad (4)$$

Where, G_k represents the generation of the turbulence kinetic energy due to the mean velocity gradients, $C_{1\varepsilon}$ *and* $C_{2\varepsilon}$ are constants. σ_k , and σ_ε are the turbulent Prandtl numbers for *k* and *ε*, respectively. S_k , *and* S_ε are user-defined source terms. ANSYS fluent provides more details information about the turbulence model [31].

4.2. Computational Schemes and Boundary Conditions

In this research, 3D models of ducted Savonius rotor had been built and validated by experimental tests. The computational domain shown in Fig. 5 is created

to solve the three-dimensional URANS. It is extended 28D in streamwise direction (x-component) 10D in vertical direction (z-coordinate) and 10D in lateral direction (y-coordinate), where D is the rotor diameter. The center of the wind turbine rotor is positioned at the middle of the spanwise distance and at 8D downstream of the inlet boundary. The extension of the computational domain is recommended by earlier researchers [30, 32-33]. The wind turbine blades, the end plates, the obstacle plate and the duct walls are dealt as no slip walls. Zero value for outlet pressure is applied at the outlet so that no differential pressure is created at the outlet. Table 1 clarifies the boundary type used for each component in the fluid domain. For the solution iterations, the time-step size varies with the rotor rotational speed 1° of rotation angle by the rotor. The computations run until the order of the convergence residuals reaches at least 10^{-5} for all solved equations except for the turbulence kinetic energy and turbulence dissipation rate equations that has an order of 10^{-4} residuals.

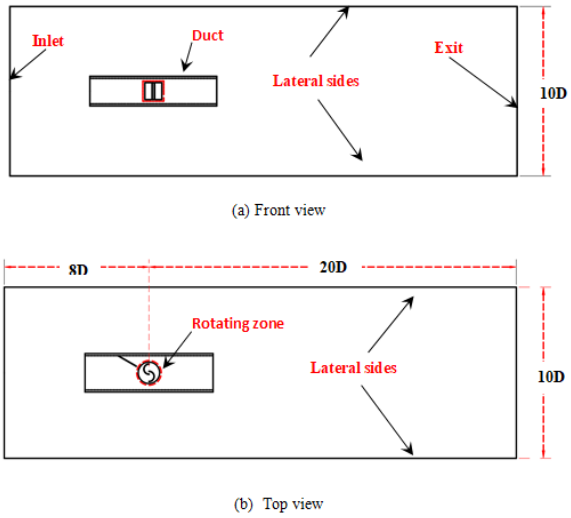

Fig. 5. Schematic representation of the computational domain (Not to scale)

Table 1 Summarized boundary conditions.

Surface	Boundary condition, type
Inlet	Inlet velocity, uniform
Top, bottom, and sides	Symmetry boundary condition
Outlet	Pressure outlet, atmospheric pressure
Rotor blades, End plates, Obstacle plates	Wall with no slip condition
Rotating zone	Moving mesh with specified RPM

ANSYS ICEM CFD software is used for meshing the computational domain. The computational grid is divided into two domains, which are stationary domain (computational model, duct), and rotational domain (Savonius turbine) for the sliding mesh model. The mesh of the second part is rotated with different rotational speeds while the other region is kept fixed, and the two regions are separated by an interface. Blending between unstructured mesh around the rotor and structured mesh for the other domain zones are used in this study as shown in Fig. This technique helps to decrease the number of elements while having a high quality mesh around the rotor. Ten prism layers are generated around the blades, which leads to maximum values of dimensionless wall distance y + less than 5 over the blades. This fine mesh region is connected to the outer coarser structured region via unstructured triangular elements in the interface.

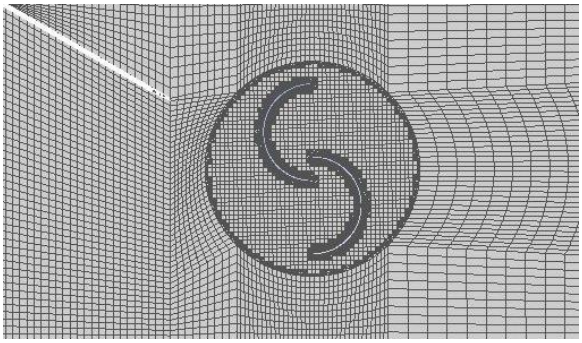

Fig. 6. Grid generation for computational domain

5. Results and Discussion

This section introduces a validation of the numerical methodology using the present measurements. Furthermore, the numerical results of the effect of obstacle flat plate installed upstream ducted Savonius turbine are also introduced. Power coefficient (C_p) of the turbine is used to reflect the characteristics of the turbine performance. The C_p is defined as the ratio of the rotor power to the available power in the oncoming wind. It is given by $C_p = \Omega T/0.5\rho A V^3$, where Ω is the angular velocity, T is the rotor torque, A is the swept area of the rotor, and V is the free-stream wind speed upstream the duct. The Savonius wind turbine is initially tested experimentally and numerically in free stream and then inside the duct. Fig. 7 introduces a comparison of C_p variation with tip speed ratio for free stream and ducted turbine. The results are obtained at two different wind speeds of 7.5 m/s and 8.7 m/s. It is noticed from the plots that there is a good agreement between the numerical results and measurements. It is also observed that the ducted turbine has better performance in terms of C_P as compared to free stream turbine. A C_{Pmax} of

0.188 is achieved ducted turbine at a wind speed of 8.7 m/s, compared with C_{Pmax} = 0.1650 for the free stream rotor. .

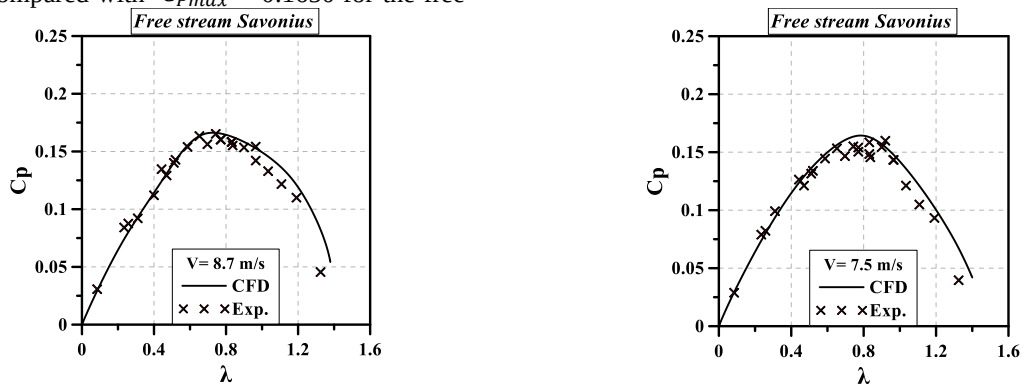

(a) Free stream Savonius turbine

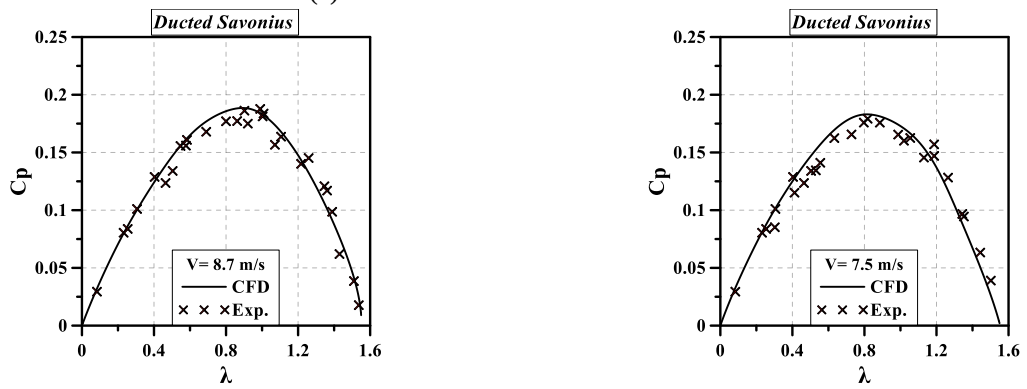

(a) Ducted Savonius turbine

Fig. 7. Comparison of present experimental and numerical results for free stream and ducted Savonius rotor

In order to explore the reasons why the improvement on the performance of Savonius turbine occurred in ducted turbine compared to free stream rotor, analysis has been employed on velocity field characteristics and pressure contours for 0º and 90º of turbine rotor angles at fixed λ for all cases. Figure 8 provides the streamlines colored by velocity contours through cross section at the center of the wind turbine rotor. It is observed that the value of velocity is maximum at tip of advancing blade and its value in case of ducted turbine is more than that of free stream turbine. Moreover, two recirculation zones are formed at the tip of advancing blade and downstream the turbine. These types of flow increase the tip losses which cause higher frictional losses, leading to reduction in produced torque. While for ducted turbine, jetting flow through the gap between the duct and turbine diminishes the appearance of recirculation zones outside the rotor swept area leading to increase in the torque and power coefficients.

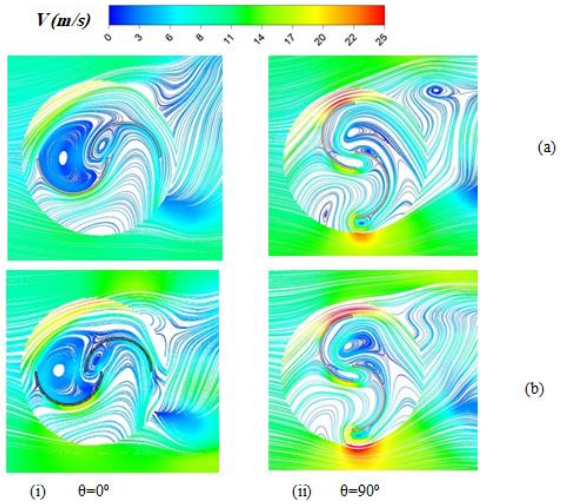

Fig. 8. Streamline colored by velocity contours for (a) un-ducted turbine (b) ducted turbine, rotor of 0º and 90º orientation angle at λ=0.8

The pressure variations through free stream turbine

and ducted one, at the same λ, are shown in Fig. 9. It is noticed that the indicated pressure is higher at the upstream of the turbine, and start to degrade behind the runner. Moreover, extensive low pressure area at the downstream of the turbines could be created in the ducted turbine, which increases the available pressure drop. The pressure drop available to the present ducted Savonius turbine depends on the flow around and through the turbine. The strong recirculation zone extended behind the runner in case of free stream condition causes a decrease in the pressure difference over the blade. This consequently leads to better performance for ducted case.

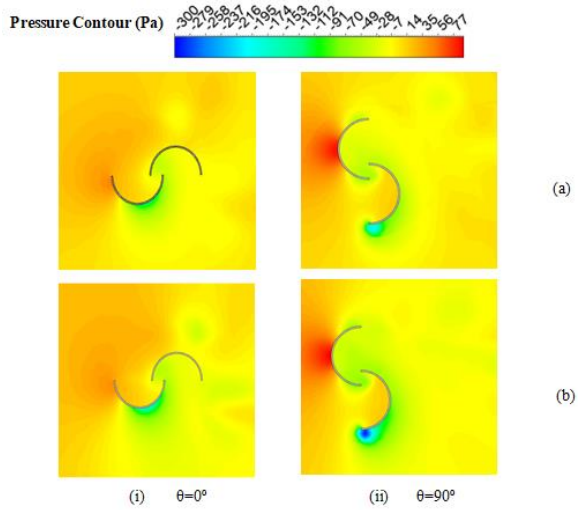

Fig. 9. Pressure contours for (a) un-ducted turbine (b) ducted turbine ,rotor of 0º and 90º orientation angle at λ=0.8

5.1. Effect of Obstacle Flat Plate Upstream the Ducted Turbine

In this section, an obstacle plate is fixed upstream a wind turbine installed in the duct. Different angles of the obstacle plate to the main flow direction are investigated numerically at the inflow wind speed of 10 m/s. The rotor performance in terms of power coefficient is presented in Fig. 10 at α=30º, 35º, and 40º along with rotor and without obstacle plate (α=0º). The tested angles showed better performance when installing any obstacle plate with the best performance of the rotor at α=35º with C_{Pmax} =0.216.

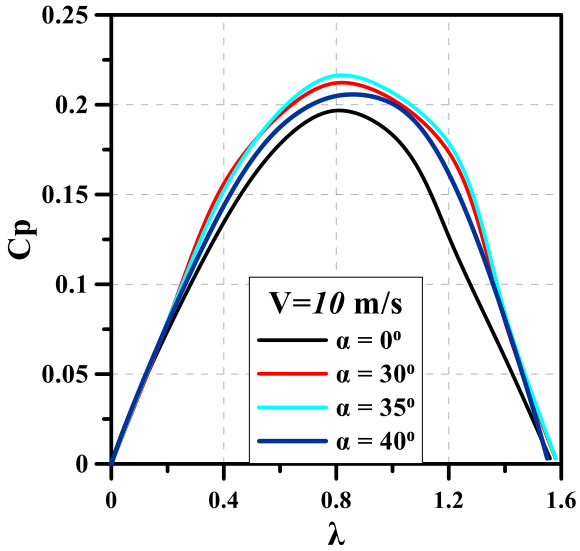

Fig. 10. Numerical results of power coefficient versus tip speed ratio for effect of obstacle flat plate upstream the ducted Savonius turbine.

The flow characteristics in terms of pressure contours and velocity contours are introduced here, to explore the effect of obstacle plate on the flow behavior around the wind turbine rotor. Figure 11 presents the pressure contour distribution for two rotor orientation of θ=0º and θ=90º at sectional top view through the rotor. The reduction in pressure behind the concave surface of the rotor increases at α= 35º but the pressure distribution for all cases is nearly similar with a slight increase in pressure drop through the rotor at α= 35º. This agrees with converge in the performance appeared in Fig. 10.

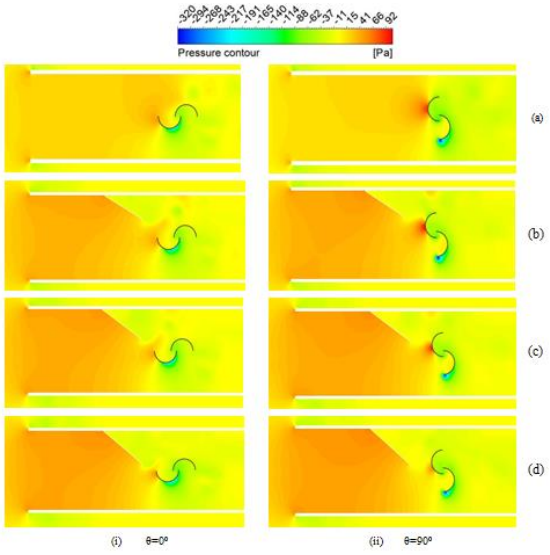

Fig. 11. Pressure contours for ducted turbine (a) α=0º, (b) α=30º, (c) α=35º, (d) α=40º , rotor of 0º and 90º orientation angle at λ=0.8.

The difference in C_p values for the four cases may be due to the flow acceleration over the concave side of the blade in the upstream. Figure 12 shows the contours for the stream wise velocity component distribution for two rotor orientations of θ=0º and θ=90º at sectional top view through the rotor. The inflow wind speed is affected by the existence of obstacle plate upstream the rotor. In case of α=30º, 35º and 40º, the resistance to the main flow increases. This leads to a decrease in the mass flow entering the duct. However, according to the continuity equation, the obstacle plate reduces the flow area which leads to enhance in the flow velocity upstream the rotor and compensation of the degradation in the flow velocity at the entering of the duct. Furthermore, the velocity magnitude appears to be slightly maximum in case of α=35º.

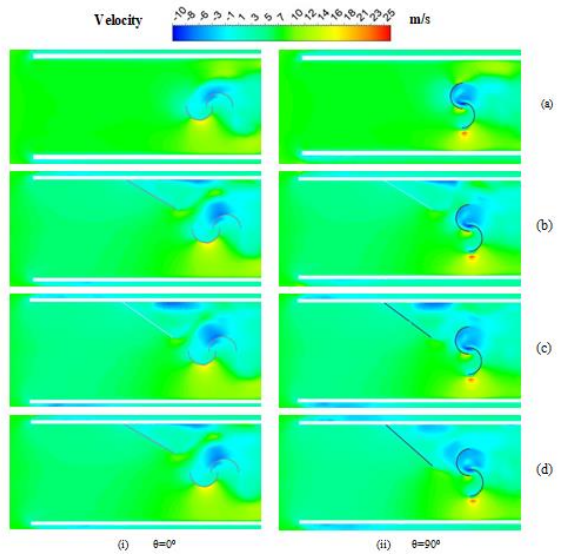

Fig. 12. Stream wise velocity component contours for ducted turbine (a) α=0º, (b) α=30º, (c) α=35º, (d) α=40º , rotor of 0º and 90º orientation angle at λ=0.8.

One important issue associated with wind turbines is the self- starting capability of the rotor. To predict this issue, the static torque exerted on the rotor at fixed rotation angles (θ) has been computed. The static torque coefficient (C_{ts}) is calculated according to the relation $C_{ts} = \frac{T_s}{0.5\rho A V^2 R}$. T_s is referred to the static torque generated on the rotor blades without rotation. Figure 13 Shows the static torque coefficient obtained for different obstacle flat plat angle (α) and free stream Savonius as a function of (θ). Due to periodicity, the results are only plotted for θ between 0º and 180º. The free stream Savonius shows large variations of the static torque with variation in rotor orientation, and in particular negative values within θ = 150º (no self-starting). Moreover, these computations demonstrate that the duct and the obstacle plate have a considerable and globally positive effect on the static torque coefficient for α=30º, 35º, with a minimum value of C_{ts} higher than around 0.03.

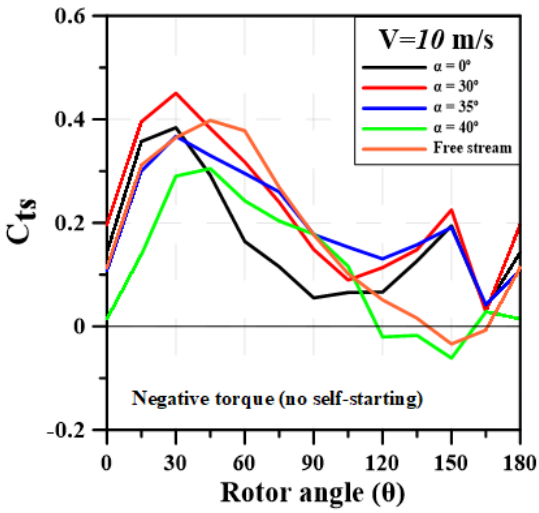

Fig. 13. Numerical results of Static torque coefficient versus rotor orientation angle at different obstacle plat angles

The rotor performance with obstacle plate of α=35º is measured experimentally and compared to the numerical results, as shown in Fig. 14. The comparison shows good agreement between the numerical predication and the experimental measurements. Hence, the present numerical methodology approves the ability to predict the performance of the rotor installed in the duct with incorporating obstacle plate upstream it.

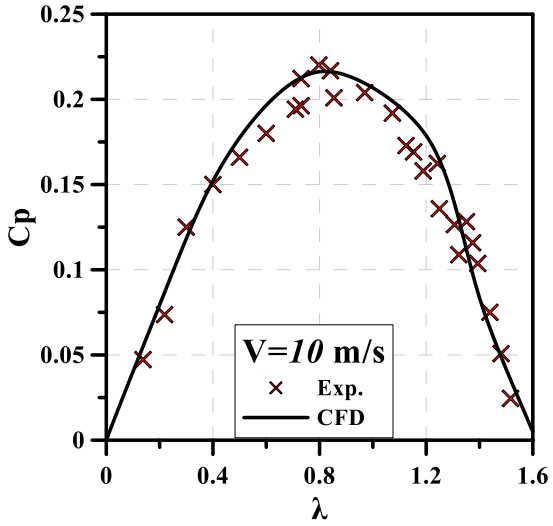

Fig. 14. Experimental and numerical results of power coefficient versus tip speed ratio for ducted Savonius turbine with obstacle flat plate α=35º.

6. Conclusion

The Savonius rotor is a promising concept for small-scale wind-energy systems, but it suffers from poor performance. Therefore, experimental and numerical investigations are carried out in the present work in order to explore the performance of the Savonius wind turbine inside a duct, prefixed with an obstacle flat plate under three orientations of the obstacle plate. The performance is compared for wind turbine rotors operating in the free wind, and in a duct with and without obstacle plates. The flow solution is obtained by 3-D URANS CFD simulations. A validation against present experimental measurements shows that the employed numerical methodology relying on the RNG k-ε turbulence model can be utilized for the prediction of the rotor performance. Moreover, the Savonius rotor installed in a duct attained higher performance levels than the free stream rotor. The installation of the obstacle plate improves the performance for the tested configurations of the obstacle plate. The overall effect of this obstacle is extremely positive for all angles, considering the obtained output power coefficient. The C_{Pmax} is found to be 0.216 at λ=0.8 and α=35º. A performance gain of 31 % is achieved over the wind turbine rotor in free wind conditions. Furthermore, considering the static torque coefficient, the installation of the obstacle improves the self-starting capability for obstacle plate angle up to α=35º. In comparison, the free stream Savonius turbine shows negative values for the static moment in some rotor orientations.

7. NOMENCLATURE

A	Rotor cross-sectional area	m^2
C_P	Power coefficient of the turbine	[-]
$C_{P_{max}}$	Maximum power coefficient of the turbine	[-]
D	Rotor rotating diameter	mm
D_o	Diameter of end plates	mm
d	Blade chord length	mm
e	Overlap distance	mm
H	Rotor height	m
k	Turbulent kinetic energy	$\frac{m^2}{s^2}$
N	Rotational speed of the rotor	rpm
P_{rotor}	Mechanical power generated by the rotor	W
V	Wind speed	$\frac{m}{s}$
w	Duct width	m
y^+	Dimensionless wall distance	[-]
ε	Turbulence dissipation rate	$\frac{m^2}{s^2}$
λ	Tip speed ratio	[-]

8- References

1. Shigetomi A., Murai Y., Tasaka Y., and Takeda Y., "Interactive flow field around two Savonius turbines", Renewable Energy (2011), Vol. 36, pp. 536–545.
2. Pope K., Dincer I., and Naterer G.F., "Energy and exergy efficiency comparison of horizontal and vertical axis wind turbines", Renewable Energy (2010), Vol. 35, pp. 2102–2113.
3. Akwa J.V., Vielmo H.A., and Petry A.P., "A review on the performance of Savonius wind turbines", Renewable and Sustainable Energy Reviews (2012), Vol. 16, pp. 3054-3064.
4. Dewan, A. Gautam, and R. Goyal, "Savonius wind turbines: A review of recent advances in design and performance enhancements", Materials Today: Proceedings (2021).
5. Al-Kayiem, H.H., Bhayo B.A., and Assadi M., "Comparative critique on the design parameters

and their effect on the performance of S-rotors", Renewable Energy (2016), Vol. 99, pp. 1306-1317.

6. Yaakob O.B., Tawi K., and Sunanto D.S., "Computer simulation studies on the effect overlap ratio for Savonius type vertical axis marine current turbine", Int. J. Eng. Trans. .Vol. 23, pp. 79-88 ,(2010)
7. Kamoji M.A., Kedare S.B., and Prabhu S.V., "Experimental investigations on single stage modified Savonius rotor", Applied Energy (2009), Vol. 86, pp. 1064-1073.
8. Jeon K.S., Jeong J.I., Pan J.K., and Ryu K.W., "Effects of end plates with various shapes and sizes on helical Savonius wind turbines", Renewable Energy (2015), Vol. 79, pp. 167-176.
9. Al-Ghriybah M., Fadhli M., Didane D.H., and Mohd S., "Review of the Recent Power Augmentation Techniques for the Savonius Wind Turbines", Journal of Advanced Research in Fluid Mechanics and Thermal Sciences (2019), Vol. 60, pp. 71-84.
10. Ogawa T., Yoshida H., and Yokota Y., "Development of rotational speed control systems for a Savonius-type wind turbine", Journal of fluids engineering (1989), Vol. 111, pp. 53-58.
11. Shaughnessy B.M., and Probert S.D., "Partially-blocked Savonius rotor", Applied Energy (1992), Vol. 4, pp. 239-249.
12. Etemadeasl, V., Esmaelnajad R., Dizaji F., and Farzaneh B., "A novel configuration for improving the aerodynamic performance of Savonius rotors", Proceedings of the Institution of Mechanical Engineers, Part A: Journal of Power and Energy (2018).
13. Iio S., Katayama Y., Uchiyama F., Sato E., and Ikeda T., "Influence of Setting Condition on Characteristics of Savonius Hydraulic Turbine with a Shield Plate", Journal of Thermal Science (2011), Vol. 20, pp. 224 - 228.
14. Kailash G., Eldho T.I., and Prabhu S.V., "Influence of the deflector plate on the performance of modified Savonius water turbine", Applied Energy (2011), Vol. 9, pp. 3207-3217.
15. Kailash G., Eldho T.I., and Prabhu S.V., "Performance Study of Modified Savonius Water Turbine with Two Deflector Plates", International Journal of Rotating Machinery (2012), Vol. 2012, Article ID 679247, 12 pages.
16. Golecha K., Eldho T.I., and Prabhu S.V., "Influence of the deflector plate on the performance of modified Savonius water turbine", Applied Energy (2011), 88, 3207–3217.
17. Aboujaoude H., Beaumont F., and Murer S., "Aerodynamic performance enhancement of a Savonius wind turbine using an axisymmetric deflector", Journal of Wind Engineering & Industrial Aerodynamics (2022), Vol. 220, pp. 104882.
18. Wahyudi B., Soeparman S., and Hoeijmakers H.W.M., "Optimization design of Savonius diffuser blade with moving deflector for hydrokinetic cross flow turbine rotor", Energy Procedia (2015), Vol. 68, pp. 244-253.
19. Roy, Sukanta, P. Mukherjee, and Saha U.K, "Aerodynamic performance evaluation of a novel Savonius style wind turbine under an oriented jet", In ASME Gas Turbine India Conference. American Society of Mechanical .Engineers, 2014
20. Altan, B.D., and Atılgan M.. "An experimental and numerical study on the improvement of the performance of Savonius wind rotor", Energy Conversion and Management (2008), Vol. 49, pp. 3425-3432.
21. El-Askary W.A., Nasef M.H., Abdel-Hamid A.A., and Gad H.E., "Harvesting wind energy for improving performance of Savonius rotor", Journal of Wind Engineering and Industrial Aerodynamics (2015), Vol. 139, pp. 8-15.
22. Mohamed M.H., Janiga G., Pap E., and Thévenin D., "Optimization of Savonius turbines using an obstacle shielding the returning blade", Renewable Energy (2010), Vol. 35, pp. 2618-2626.
23. Mohamed M.H., Janiga G., Pap E., and Thévenin D., "Optimal blade shape of a modified Savonius turbine using an obstacle shielding the returning blade", Energy Conversion and Management (2011), Vol. 52, pp. 236–242.
24. Hansen M.O.L., Sørensen N.N., and Flay R.G.J., "Effect of placing a diffuser around a wind

turbine", Wind Energy (2000), Vol. 3, pp. 207–213.

25. Lawn J., "Optimization of the power output from ducted", Proceedings of the institution of mechanical engineers, Part A, Journal of Power and Energy (2003), 217.
26. Mishra N., Jain A., Nair A., Khanna B., and Mitra S., "Experimental investigation on a ducted Savonius vertical axis wind turbine and its Performance Comparison with and without end plates", RERA (2020), Vol. 1, pp. 1-9.
27. Bai H.L., Chan C.M., Zhu X.M., and Li K.M., "A numerical study on the performance of a Savonius-type vertical-axis wind turbine in a confined long channel", Renewable Energy (2019), 139, pp. 102-109.
28. Mauro S., Brusca S., Lanzafame R., and Messina M., "CFD modeling of a ducted Savonius wind turbine for the evaluation of the blockage effects on rotor performance", Renewable Energy (2019), 141, pp. 28-39.
29. El-Askary W.A., Saad A.S., AbdelSalam A.M., and Sakr I., "Investigating the Performance of a Twisted Modified Savonius Rotor", Journal of Wind Engineering and Industrial Aerodynamics (2018), Vol. 182, pp. 344–355.
30. AbdelSalam A.M., El-Askary W.A., Kotb M.A., and Sakr I.M., "Experimental study on small scale horizontal axis wind turbine of analytically-optimized blade with linearized chord twist angle profile", Energy (2021), Vol. 216, pp. 119304.
31. Fluent, ANSYS FLUENT 17.0 User's Guide (2017).
32. Lee, J. H., Lee, Y. T., and Lim, H. C., 2016, "Effect of Twist Angle on the Performance of Savonius Wind Turbine", Renewable Energy, Vol. 89, pp. 231–244.
33. El-Askary W.A., Saad A.S., AbdelSalam A.M., and Sak I.M., "Experimental and Theoretical Studies for Improving the Performance of a Modified Shape Savonius Wind Turbine", Journal of Energy Resources Technology, Transactions of the ASME, (2020), 142(12): 121303.